

# Synthesis and Characterization of Yttria-Stabilized Zirconia (YSZ) Nano-Clusters for Thermal Barrier Coatings (TBCs) Applications

Satish Tailor<sup>1</sup> · Manoj Singh<sup>2</sup> · A. V. Doub<sup>1</sup>

Received: 26 March 2016 / Published online: 22 April 2016  
© Springer Science+Business Media New York 2016

**Abstract** Yttria-stabilized zirconia (YSZ) nano-clusters were synthesized by a sol–gel process. The aim was to produce YSZ powders in order to prepare thick coatings for thermal barrier to be applied on gas turbine engine components. Yttrium nitrate hexahydrate and zirconium oxy-chloride octahydrate were used as a source of zirconium, citric acid was taken as a chelating agent, and ethylene glycol was used as a polyesterification agent. The synthesized powders were characterized by X-ray diffraction, transmission electron microscopy, thermo-gravimetric analysis and differential scanning calorimetry, and Raman spectroscopy. Furthermore, parameters were critically analyzed in order to synthesize non-transformable (*t'*) tetragonal crystal structure, which is the best zirconia phase for high temperature thermal barrier coatings applications. In this regard, tetragonal YSZ nano-clusters were heated in an alumina crucible at a temperature of 1200 °C for 100 h.

**Keywords** Ceramic · Nano-cluster · Yttria-stabilized zirconia · Thermal barrier coating

## Introduction

Yttria-stabilized zirconia (YSZ) ceramic nano-clusters have wide range of specific important properties such as high strength, high ionic conductivity, low thermal conduction, chemical inertness, high chemical and thermal stability, and high refractive index [1–4], and are attractive for many applications such as high-

---

✉ Satish Tailor  
dr.saty@yahoo.in

<sup>1</sup> Department of Protection of Metal and Surface Technology, National University of Science and Technology “MISIS”, Leninsky Prospect, 4, Moscow, Russia 119049

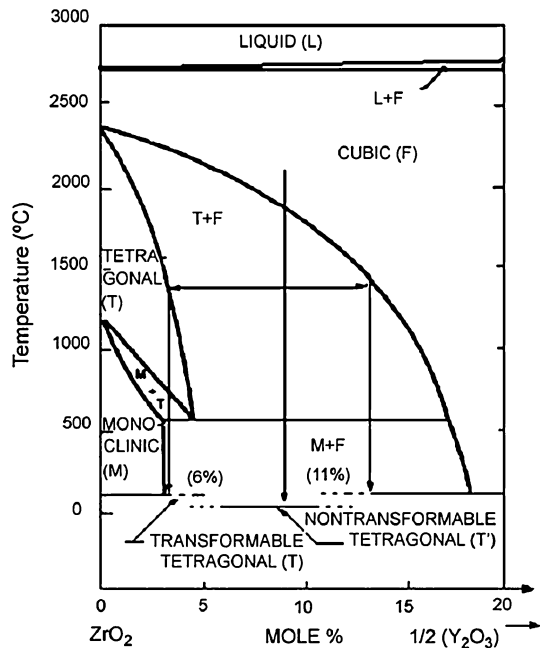
<sup>2</sup> Laboratory of Biomedical Nanomaterials, National University of Science and Technology “MISIS”, Leninsky Prospect, 4, Moscow, Russia 119049

temperature thermal barrier coatings (TBCs) applications [5], fuel cells [6, 7], catalysis [8–10], sensors [11, 12], bioseparation [13], and chromatography [14–17].

Besides the all these applications, YSZ ceramic nano-clusters have considerable attention for the high-temperature TBCs application (gas turbine engine application) in the last 5 years. At room pressure, zirconia has three phases including cubic, tetragonal, and monoclinic depending on the range of temperature [18]. For the high-temperature TBCs application tetragonal phase is found to be most suitable [19]. To keep the tetragonal phase metastable at room temperature is different in terms of the undoped zirconia crystallite size. Tetragonal phase of zirconia is thermodynamically a metastable phase at low temperatures and it changes into equilibrium phases at elevated temperatures [20, 21].

The transformable (t) tetragonal zirconia phase shows high hardness and strength which makes it appropriate material for use as engineering ceramic material because the tetragonal (t) phase structure transforms into a monoclinic phase which gives it high mechanical strength [22, 23]. This phase transformation could be helpful in certain respects for engineering ceramic materials. However, because of this phase transformation a number of static damages occurs in the results due to about 4.5 % volume expansion at high temperatures, this phase transformation particularly limits the usage of tetragonal (t) zirconia material at elevated temperatures such as a thermal barrier coating (TBC), which depends on the durability, stability at high-temperature and very low thermal conductivity [19]. However, the ‘non-transformable’ metastable tetragonal YSZ phase (called t’) [24] is perfectly resistant and does not transform to the monoclinic phase under the physical stresses or thermal

**Fig. 1**  $ZrO_2$ – $Y_2O_3$  phase diagram, after Miller et al. [26]



cycling stresses. The  $t'$  phase is recognized as the most suitable and used for TBC applications due to the formation of a specific microstructure (called tweed) which leads to increase the thermo-mechanical performances [25]. This microstructure corresponds to a three-dimensional pseudo-periodic lattice of high  $Y_2O_3$  cubic particles within all of the  $t'$  grains. However, as Miller et al. [26] first reported,  $t'$  phase undergoes a phase separation by diffusion when aged at temperatures greater than 1200 °C which can allow the tetragonal to monoclinic transformation upon cooling.

In the case of YSZ, the volume of yttrium is an important factor for the fabrication of the metastable tetragonal phases. According to the phase diagram proposed by the Miller et al. [26] (Fig. 1), the domain of existence of the  $t$  phase,  $t$ , is in the range 0–6 mol%  $YO_{1.5}$ . The more addition of the yttrium volume to the zirconia permits to get the ' $t'$ ' phase up to about 13 mol%  $YO_{1.5}$  [26]. A study has been done in National Aeronautics and Space Administration (NASA) research reports that the best spalling performance and thermal cycle life occurred at 6.8–9.0 wt%  $Y_2O_3$  [27, 28].

In this study, YSZ nano-clusters with metastable  $t'$  phase were synthesized by a chemical route known as sol–gel method. The objective was to determine if the sol–gel route was able to synthesize YSZ powders with the same metastable tetragonal crystal structure ( $t'$ ) like conventional physical processes would be able to do so [29]. In order to determine possible different crystal structures of the final product precisely, investigations by X-ray diffraction and Raman spectroscopy were carried out. The thermal behavior of the precursor gel was investigated by thermogravimetric analysis and differential scanning calorimetry. Finally, the morphology and particle size of the final product were characterized by means of field emission scanning electron microscope and transmission electron microscopy.

## Experimental

### Synthesis of YSZ Nano-Clusters

Based on simple sol–gel method [30], the YSZ nano-clusters were synthesized using citric acid chelates with a wide range of cations. After the addition of ethylene glycol and heating, the chelate was transformed into a polymer with a homogeneous cation distribution. Yttrium nitrate hexahydrate and Zirconium oxychloride were used as raw materials. Yttrium salt, zirconium salt and citric acid solutions were prepared by using the raw materials with distilled water. Further mixing and heating on a hot plat stirrer and adding ethylene glycol with an aqueous concentrate under heating and stirring. Quite enough quantities of Y and Zr solutions were mixed and make homogeneous concentration by stirring at 100 and 200 °C. The molar ratios as 1:4 were used of citric acid: ethylene glycol and citric acid: metal, respectively. The pure YSZ was synthesized from the metal citrate complex polyesterified in ethyleneglycol. By the heating at temperature 300 °C most of the organic materials were subsequently eliminated, and a brown residue containing reactive oxides with well-controlled stoichiometry was formed. The formed porous product was crushed

and heated in an alumina crucible to 1200 °C for 100 h to crystallize the YSZ nano-clusters.

### Characterization of YSZ Nano-Clusters

By the two techniques, Differential scanning calorimetry (DSC, Netzsch STA 449C) and the thermogravimetric analysis (STA NET-ZSCH409 PC/PG), the thermal behavior of YSZ nano-clusters gel was examined using 5 mg powder of the dried clusters heating from the room temperature to 600 °C under the air atmosphere at the rate of 10 °C/min.

The Fourier transform infrared spectroscopy (FT-IR) spectra were recorded between 4000 and 400  $\text{cm}^{-1}$  with a resolution of 1  $\text{cm}^{-1}$  using KBr pellets that had 25 wt% of YSZ nano-clusters.

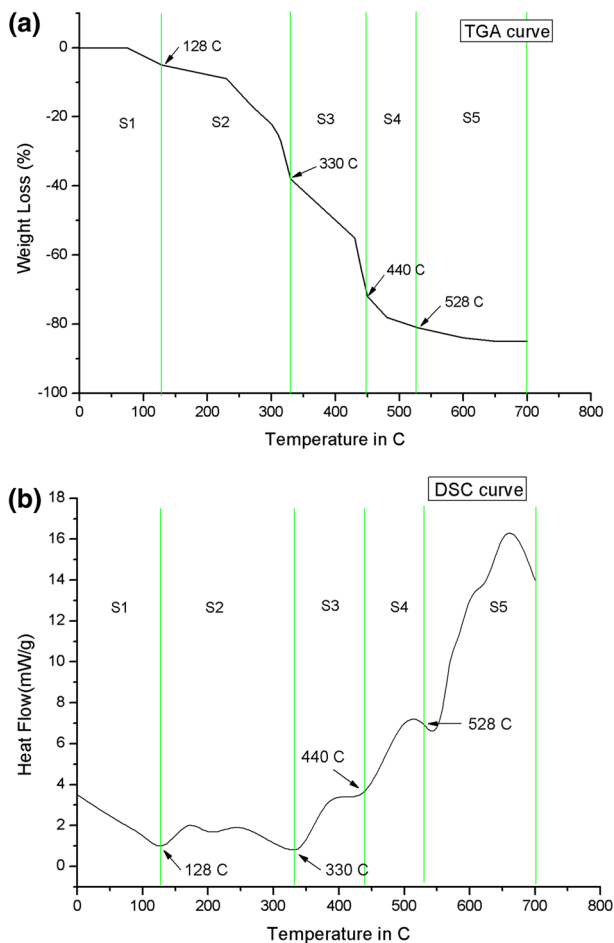


**Fig. 2** TGA (a) and DSC (b) curves for YSZ burned nano-clusters at the rate of 5 °C/min

Phase analysis of the YSZ nano-clusters was done by an X-ray diffraction XRD (D8 ADVANCE, Bruker, Germany) using Cu  $k\alpha$  radiation ( $\lambda = 0.15406$  nm) produced at 40 kV and 40 mA. The analyzed range of the diffraction angle  $2\theta$  was between  $20^\circ$  and  $90^\circ$ , by step width of  $0.03^\circ$  and a time per step equal to 1 s. Crystalline size of the nano-clusters was estimated by the Scherrer formula, as given in the following equation [31].

$$D = K\lambda/b \cos \theta \quad (1)$$

where  $D$  is the crystallite size of the YSZ nano-clusters,  $b$  is the width at half maximum (FWHM) of a Bragg peak,  $K$  is the X-ray wavelength and  $\lambda$  is the Bragg angle.

Raman spectra were measured on YSZ nano-clusters at  $100\text{--}800$   $\text{cm}^{-1}$  by Raman Microscope (BRUKER, SENTERRA, Germany). The spectral excitation was provided by an  $\text{Ar}^+$  laser, using the 785 nm line.

The morphology and particle size of YSZ nano-clusters were determined using transmission electron microscopy (TEM, H700H, Hitachi), which operated at 200 kV voltage conditions.

## Results and Discussion

### Thermal Analysis

The TGA and DSC curves of YSZ nano-clusters are presented in Fig. 2. Crystallization, oxidation, dehydration, combustion and are the most significant thermal reactions perceived [32]. In four stages the overall total weight loss was about 85 % of the total mass.

The first weight loss was noted at the temperature range of  $100\text{--}128$   $^\circ\text{C}$  that corresponded to the first endothermic peak shown by DSC curve. That could be because of the evaporation of the absorbed water. The second weight loss was noted at the temperature range of  $200\text{--}330$   $^\circ\text{C}$ . The third and fourth stages, which were noted in the temperature ranges of  $330\text{--}440$  and  $430\text{--}528$   $^\circ\text{C}$  respectively, could be attributed to the degradation of organic compounds. The third weight loss, in the range of  $330\text{--}440$   $^\circ\text{C}$  shown by TGA curve, corresponding DSC curve at  $440$   $^\circ\text{C}$  could be related to the decomposition of the organo-metallic compounds that were formed by hydrolysis and condensation of the nano-clusters and/or could be related to the carbon dioxide removal and the destruction of the polymeric nano-clusters network [33, 34]. The fourth weight loss, corresponding to the DSC curve (endothermic peak) at the temperature range of  $430\text{--}528$   $^\circ\text{C}$  might be attributed to the carbonization or bond breaking of residue organic moieties in precursors [33–35].

### FTIR Analysis

Infrared vibrational spectra of burned YSZ nano-clusters and the final product after heat treatment at  $1200$   $^\circ\text{C}$  for 100 h are shown in Fig. 3a, b respectively. These

absorption spectra of the infrared rays are used to identify the functional groups of the organic compounds. Several peaks at resin or burned gel were observed in the FTIR spectrum (Fig. 3a). The observed bands at 1800, 1650 and 1400  $\text{cm}^{-1}$  could be assigned to the carboxylate stretching vibrations. Bands in 1800  $\text{cm}^{-1}$  could be related to the stretching mode of C=O esteric groups made by polymerization of citric acid and ethylene glycol. Bands at 1400 and 1650  $\text{cm}^{-1}$  might be the symmetric and asymmetric stretching vibrations of the carboxylate group. The difference between symmetric and asymmetric stretching vibration ( $V_{\text{as}} - V_{\text{s}}$ ) was equal to 250  $\text{cm}^{-1}$ , indicates that there was a complex formed by a reaction between citric acid and metal ions (Zr and Y ions) [36]. Bands in 1150  $\text{cm}^{-1}$  could correspond to the COH group and bands lower than the 800  $\text{cm}^{-1}$  might be the metal–oxygen stretching mode caused by the connection between citric acid and metal ions. The broad peak in the 3500  $\text{cm}^{-1}$  could be assigned to the stretching mode of O–H [37].

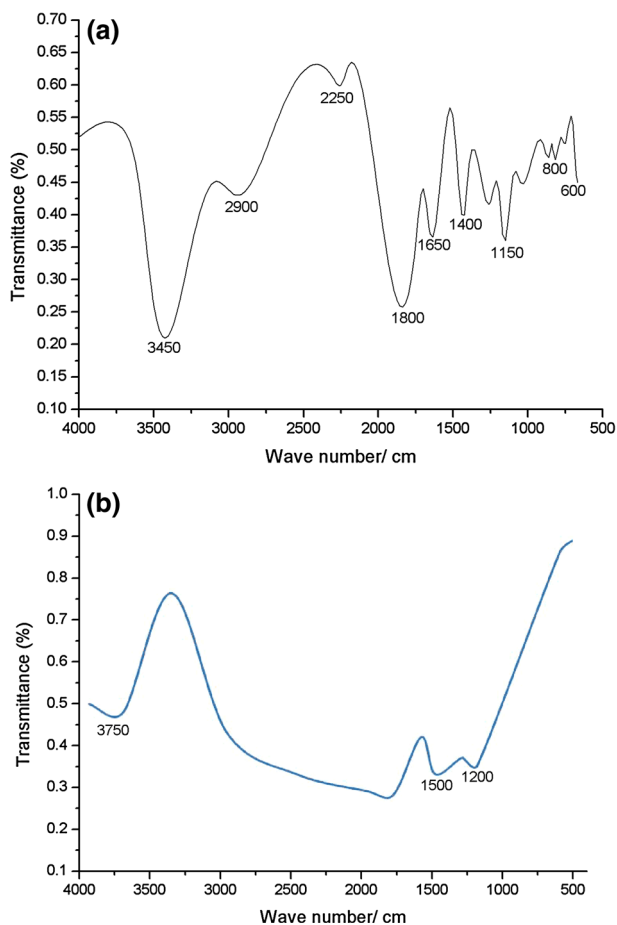


**Fig. 3** FT-IR spectra of **a** burned YSZ nano-clusters and **b** the final product after heat treatment at 1200 °C for 100 h

According to Fig. 3b, after heat treatment of YSZ nano-clusters at the temperature of 1200 °C, the peaks related to the carbon skeletons and carboxylate anions in the nano-clusters gel were almost eliminated. Nonetheless, the very low band peaks related to symmetric and asymmetric stretching vibrations of the carboxylate groups (at 1500 and 1200  $\text{cm}^{-1}$ ) which might be assigned to the presence of the organics obtained from the YSZ nano-clusters gel decomposition that could be adsorbed on the particles surface and prevent the aggregation of the nano-clusters. The band at 3750  $\text{cm}^{-1}$  could be related to the asymmetric vibrational frequencies of the Zr-OH [38–40].

### XRD Analysis of YSZ Nano-Clusters

YSZ nano-clusters were annealed at 1200 °C for period of 100 h in air using an alumina crucible. Nano-clusters were then cooled overnight at 10 °C  $\text{min}^{-1}$  cooling rates (or lower) and then sample was characterized by XRD. The obtained XRD patterns are shown in Fig. 4 indicated the formation of a single-crystalline tetragonal phase. Even after a period of 100 h at 1200 °C, the tetragonal phase was still pure and no monoclinic (cubic) phase was observed under the detection level. Furthermore, the crystallite size of YSZ nano-clusters was calculated by Sherrer equation and found to be 30 nm.

### Raman Spectroscopy of YSZ Nano-Clusters

The monoclinic symmetry of zirconia has four molecules per unit cell and eighteen Raman active modes and the tetragonal symmetry of zirconia has two molecules per unit cell and six Raman active modes [45, 46]. The cubic symmetry with fluorite symmetry has four molecules per unit cell and only one Raman active mode [45,

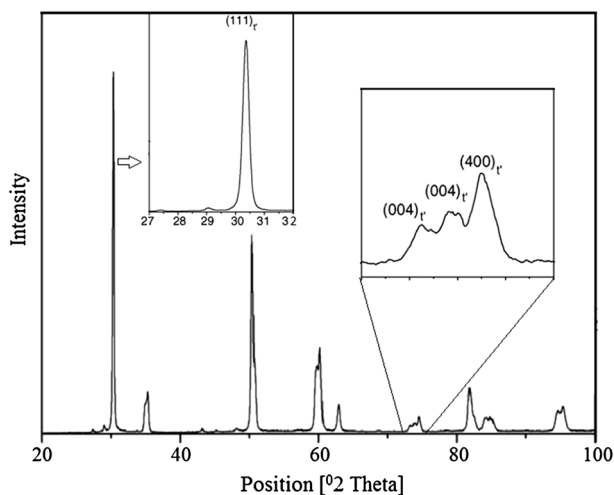


**Fig. 4** XRD patterns of YSZ nano-clusters after heat treatment at 1200 °C for 100 h

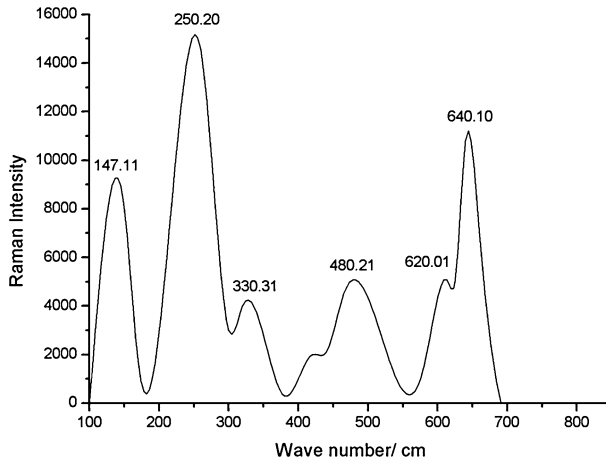


**Fig. 5** Raman spectra of YSZ nano-clusters showing tetragonal ( $t'$ ) structure

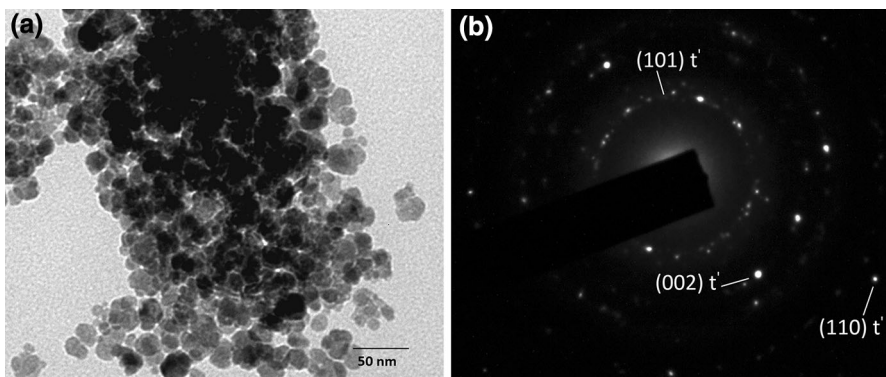


**Fig. 6** **a** TEM micrographs and **b** electron diffraction patterns of YSZ heat treated at 1200 °C for 100 h showing tetragonal  $ZrO_2$

46]. Raman spectrum of the YSZ nano-clusters is shown in Fig. 5, clearly indicating six bands confirming that the structure of zirconia was tetragonal. Same kind of results have been reported by other authors, as most of the bands were observed near at 250 and 640  $cm^{-1}$  and used as an indication of the tetragonal structure [41–46].

### YSZ Nano-Clusters Characterization by TEM

TEM micrographs, as shown in Fig. 6, clearly indicated that the sizes of the synthesized YSZ nano-clusters were in the nano range. It can be observed that the agglomerated nano-clusters, also have a fine crystallites and all are uniform in the size and shapes. From the TEM images (Fig. 6a), the average particle size for the YSZ nano-clusters was found to be 40 nm. The electron diffraction patterns



(Fig. 6b) clearly revealed the ring patterns of polycrystalline tetragonal zirconia phase.

## Conclusions

YSZ nano-clusters were successfully fabricated by the simple chemical sol–gel method in order to prepare thick coatings for thermal barrier to be applied on gas turbine engine components. The synthesized YSZ nano-clusters were characterized by TG, DSC, FT-IR XRD, Raman spectroscopy and TEM in order to evaluate the crystal structure, thermal behavior and morphological assessment of the final nano-clusters produced by this method. Crystal structure investigations by XRD and Raman spectroscopy showed that non-transformable tetragonal crystal structure of zirconia, which was desirable for TBC's, could be fabricated by this approach. Transmission electron microscopy of YSZ nano-clusters confirmed the average particle size was 40 nm with broad particle size distribution. The synthesis approach of nano-clusters by this method might be used to achieve the better thermal insulation to the gas turbine engine components at the higher operating temperature by developing a TBC.

**Acknowledgments** The authors gratefully acknowledge the financial support of the Ministry of Education and Science of the Russian Federation in the framework of Increase Competitiveness Program of NUST «MISiS» (Grant No. K4-2014-081) and experimental support of National University of Science and Technology “MISiS”, Moscow, Russia.

## References

1. L. Kumari, W. Li, J. Xu, R. Leblanc, D. Wang, Y. Li, H. Guo, and J. Zhang (2009). Controlled hydrothermal synthesis of zirconium oxide nanostructures and their optical properties. *Cryst. Growth Des.* **9**, (9), 3874–3880.
2. I. Freris, P. Riello, F. Enrichi, D. Cristofori, and A. Benedetti (2011). *Opt. Mater.* **33**, 1745–1752. doi:10.1016/j.optmat.2011.06.010.
3. J. He, J. Chen, L. Ren, Y. Wang, C. Teng, M. Hong, et al. (2014). *ACS Appl. Mater. Interfaces* **6**, 2718–2725. doi:10.1021/am405202d.
4. H. Uchiyama, K. Takagi, and H. Kozuka (2012). *Colloids Surf. A Physicochem. Eng. Asp.* **403**, 121–128. doi:10.1016/j.colsurfa.2012.03.065.
5. D. R. Clarke and C. G. Levi (2003). *Annu. Rev. Mater. Res.* **33**, 383–417. doi:10.1146/annurev.matsci.33.011403.113718.
6. T. Koch and P. Ziemann (1996). *Appl. Surf. Sci.* **99**, 51–57. doi:10.1016/0169-4332(95)00512-9.
7. J. H. Shim, C. Chao, H. Huang, and F. B. Prinz (2007). *Chem. Mater.* **19**, 3850–3854. doi:10.1021/cm070913t.
8. T. Miller and V. Grassian (1995). *J. Am. Chem. Soc.* **117**, 10969–10975. doi:10.1021/ja00149a020.
9. Y. Li, D. He, Z. Cheng, C. Su, J. Li, and Q. Zhu (2001). *J. Mol. Catal. A Chem.* **175**, 267–275. doi:10.1016/S1381-1169(01)00233-3.
10. D. Chen, L. Cao, F. Huang, P. Imperia, Y.-B. Cheng, and R. A. Caruso (2010). *J. Am. Chem. Soc.* **132**, 4438–4444. doi:10.1021/ja100040p.
11. D. Lu, J. Wang, L. Wang, D. Du, C. Timchalk, R. Barry, et al. (2011). *Adv. Funct. Mater.* **21**, 4371–4378. doi:10.1002/adfm.201100616.
12. M. Zhou and A. Ahmad (2006). *Mater. Res. Bull.* **41**, 690–696. doi:10.1016/j.materresbull.2005.10.018.

13. A. Subramanian, P. W. Carr, and C. V. McNeff (2000). *J. Chromatogr. A* **890**, 15–23. doi:10.1016/S0021-9673(00)00289-2.
14. B. Yan, C. McNeff, and F. Chen (2001). *J. Am. Ceram. Soc.* **27**, 1721–1727. doi:10.1111/j.1151-2916.2001.tb00905.x.
15. B. Yan, C. V. McNeff, P. W. Carr, and A. V. McCormick (2005). *J. Am. Ceram. Soc.* **88**, 707–713. doi:10.1111/j.1551-2916.2005.00133.x.
16. A. Pattanayak and A. Subramanian (2009). *Powder Technol.* **192**, 359–366. doi:10.1016/j.powtec.2009.01.023.
17. A. Pattanayak and A. Subramanian (2011). *Int. J. Appl. Ceram. Technol.* **8**, 94–111. doi:10.1111/j.1744-7402.2009.02410.x.
18. H. Liu, H. Jazi, M. Bussmann, and J. Mostaghimi (2009). Experiments and modeling of rapid solidification of plasma-sprayed yttria-stabilized zirconia. *Acta Mater.* **57**, (20), 6013–6021.
19. C. Viazzi, J.-P. Bonino, F. Ansart, and A. Barnabé (2008). Structural study of metastable tetragonal YSZ powders produced via a sol–gel route. *J. Alloys Compd.* **452**, (2), 377–383.
20. G. Stefanic, S. Music, B. Grzeta, S. Popovic, and A. Sekulic (1998). Influence of pH on the stability of low temperature t-ZrO<sub>2</sub>. *J. Phys. Chem. Solids* **59**, (6), 879–885.
21. G. Pacheco and J. Fripiat (2000). Physical chemistry of the thermal transformation of mesoporous and microporous zirconia. *J. Phys. Chem. B* **104**, (50), 11906–11911.
22. I. Nettleship and R. Stevens (1987). Tetragonal zirconia polycrystal (TZP)—a review. *Int. J. High Technol. Ceram.* **3**, (1), 1–32.
23. E. Subbarao (1981). Ceramic dielectrics for capacitors. *Ferro-electrics* **35**, (1), 143–148.
24. H. Scott (1975). Phase relationships in the zirconia-yttria system. *J. Mater. Sci.* **10**, (9), 1527–1535.
25. R. Mevrel, C. Rio, M. Poulain, C. Diot, and F. Nardou (1987). Technical Report No. 28/2019M. ONERA.
26. R. A. Miller, J. L. Smialek, and R. G. Garlick (1981). Phase stability in plasma-sprayed, partially stabilized zirconia-yttria. *J. Am. Ceram. Soc.* **3**, 241.
27. R. A. Miller (1997). Thermal barrier coatings for aircraft engines: history and directions. *J. Therm. Spray. Technol.* **6**, (1), 35–42.
28. S. Bose *High temperature coatings* (Butterworth-Heinemann, UK, 2011).
29. C. Viazzi, F. Ansart, and J. P. Bonino *Proceeding of the Poudres et Matériaux Frittes 2005* (Cherbourg, France, 2005).
30. M. Pechini (1967). Patent No. 3,330,697. United States Patent Office.
31. B. D. Cullity and S. R. Stock *Elements of X-ray diffraction*, vol. 3 (Prentice Hall Upper Saddle River, NJ, 2001).
32. R. S. da Silva, M. I. B. Bernardi, and A. C. Hernandez (2007). Synthesis of non-agglomerated Ba<sub>0.77</sub>Ca<sub>0.23</sub>TiO<sub>3</sub> nanopowders by a modified polymeric precursormethod. *J. Sol-Gel Sci. Technol.* **42**, (2), 173–179.
33. K. Singh, L. Pathak, and S. Roy (2007). Effect of citric acid on the synthesis of nano-crystalline yttria stabilized zirconia powders by nitrate–citrate process. *Ceram. Int.* **33**, (8), 1463–1468.
34. S. Sakka *Handbook of sol-gel science and technology. I. Sol-gel processing*, vol. 1 (Springer, New York, 2005).
35. M. Kakihana and M. Yoshimura (1999). Synthesis and characteristics of complex multicomponent oxides prepared by polymer complex method. *Bull. Chem. Soc. Jpn.* **72**, (7), 1427–1443.
36. Y. Xu, X. Yuan, G. Huang, and H. Long (2005). Polymeric precursor synthesis of Ba<sub>2</sub>Ti<sub>9</sub>O<sub>20</sub>. *Mater. Chem. Phys.* **90**, (2), 333–338.
37. G. Socrates and G. Socrates *Infrared and Raman characteristic group frequencies: tables and charts* (Wiley, Chichester, 2001).
38. Y. Zhang, A. Li, Z. Yan, G. Xu, C. Liao, and C. Yan (2003). (ZrO<sub>2</sub>)<sub>0.85</sub>(REO<sub>1.5</sub>)<sub>0.15</sub>. *Res. J. Solid State Chem.* **171**, (1–2), 434–438.
39. C. Laberty-Robert, F. Ansart, C. Deloget, M. Gaudon, and A. Rousset (2001). Powder synthesis of nanocrystalline ZrO<sub>2</sub>–8 % Y<sub>2</sub>O<sub>3</sub> via a polymerization route. *Mater. Res. Bull.* **36**, (12), 2083–2101.
40. Y.-W. Zhang, Z.-G. Yan, F.-H. Liao, C.-S. Liao, and C.-H. Yan (2004). Citrate gel synthesis and characterization of (ZrO<sub>2</sub>)<sub>0.85</sub>(REO<sub>1.5</sub>)<sub>0.15</sub> (RE = Y, Sc) solid solutions. *Mater. Res. Bull.* **39**, (11), 1763–1777.
41. D. Thackeray (1974). The Raman spectrum of zirconium dioxide. *Spectrochimica Acta A Mol. Spectrosc.* **30**, (2), 549–550.
42. C. Li and M. Li (2002). UV Raman spectroscopic study on the phase transformation of ZrO<sub>2</sub>, Y<sub>2</sub>O<sub>3</sub>–ZrO<sub>2</sub> and SO<sub>4</sub><sup>2-</sup>/ZrO<sub>2</sub>. *J. Raman Spectrosc.* **33**, (5), 301–308.

43. A. Naumenko, N. Berezovska, M. Biliy, and O. Shevchenko (2008). Vibrational analysis and Raman spectra of tetragonal zirconia. *Phys. Chem. Solid State* **9**, (1), 121–125.
44. D. Gazzoli, G. Mattei, and M. Valigi (2007). Raman and X-ray investigations of the incorporation of  $\text{Ca}^{2+}$  and  $\text{Cd}^{2+}$  in the  $\text{ZrO}_2$  structure. *J. Raman Spectrosc.* **38**, (7), 824–831.
45. C. Perry, D. W. Liu, and R. P. Ingel (1985). Phase characterization of partially stabilized zirconia by Raman spectroscopy. *J. Am. Ceram. Soc.* **68**, (8), C184–C187.
46. D. J. Kim, H. J. Jung, and I. S. Yang (1993). Raman spectroscopy of tetragonal zirconia solid solutions. *J. Am. Ceram. Soc.* **76**, (8), 2106–2108.